Optics Communications 546 (2023) 129773

Contents lists available at ScienceDirect

Optics Communications

journal homepage: www.elsevier.com/locate/optcom

Control and stabilization of Kerr cavity solitons and breathers driven by chirped optical pulses

Francesco Rinaldo Talenti [a,*], Yifan Sun [a], Pedro Parra-Rivas [a], Tobias Hansson [b], Stefan Wabnitz [a,c]

[a] Dipartimento di Ingegneria dell'Informazione, Elettronica e Telecomunicazioni, Sapienza University of Rome, Via Eudossiana, 18, Roma, 00184, Italy
[b] Department of Physics, Chemistry and Biology, Linköping University, Linköping, SE-581 83, Sweden
[c] CNR-INO, Istituto Nazionale di Ottica, Via Campi Flegrei, 34, Pozzuoli, 80078, Italy

ARTICLE INFO

Keywords:
Temporal solitons
Optical frequency combs
Kerr effect
Dissipative structures

ABSTRACT

We investigate the impact of chirped driving fields on the dynamics and generation of Kerr cavity breathers and solitons. Synchronous phase and amplitude modulation of the pumping field can be exploited in order to control soliton dynamics. Here we show that using a phase-modulated super-Gaussian pump permits to stabilize the oscillations of breathing solitons. Moreover, our scheme permits to obtain new dynamical attractors, with a prescribed temporal intra-cavity pattern. Straightforward applications are the deterministic generation of optical frequency soliton combs, optical tweezers, and more generally, all-optical manipulation of light pulses.

1. Introduction

Temporal cavity solitons (CSs) are self-sustained light pulses, which propagate unchanged thanks to the compensation of chromatic dispersion by the Kerr effect on the one hand, and of cavity loss by coherent injection of an external pump on the other hand [1]. CSs received a great deal of attention in recent years, because of their potential applications, e.g., to all-optical buffering [2], optical communications [3], dual-comb spectroscopy [4], optical tweezers [5] and, more generally, to light manipulation [6]. Remarkably, in the frequency domain, a CS forms a coherent optical frequency comb (OFC): scattering of a CS into dispersive waves may lead to octave-spanning OFCs, thus enabling an integrated optical platform for self-referenced optical laser sources [7].

Spatial CSs have first been demonstrated in VCSELs [6], whereas temporal CSs have been generated in fiber loop resonators [2] and, more recently, in microresonators [8]. Although CSs are typically pumped by a continuous wave (CW) external laser, a synchronous pulse train may also be used [9,10]. With a pulsed pump, the CS is naturally generated on the top of the pump temporal intensity profile [10]. However, by using specific amplitude [11,12] or phase [13–16] pump modulation schemes, one may push the soliton away from the center of the pump pulse. In general, appropriate shaping of the pump pulses may enable to control the generation of robust temporal dissipative structures or dynamical attractors [17]. In the context of optical communications, the control of soliton dynamics has been extensively investigated. A method for suppressing soliton interactions is based on synchronously driving the phase profile of a soliton pulse train, which can be implemented by means of periodic phase modulation [18,19]. It was demonstrated that the use of a phase modulator leads to noise suppression and timing jitter reduction [20]. More generally, pulse shaping techniques can be used for retiming functionalities in return-to-zero (RZ) signal regeneration techniques [21]. Recently, the generation of breathing solitary waves, or breathers, in passive Kerr resonators has been investigated, both theoretically and experimentally [22–24]. The resulting dynamics unveiled unexplored physics, where the intracavity field has a finite amplitude oscillation around a CS state. The resulting rich spatiotemporal dynamics may be controlled by acting on different key parameters, possibly leading to convergence of the cavity output field towards a physical state of interest. In [22,25], for instance, it has been shown how the insertion of a parabolic potential allows for the stabilization of chaotic or oscillatory dynamics, triggering the generation of periodic temporal patterns. In this communication, we propose and theoretically demonstrate that a chirped phase modulation of a time-dependent driving pump field permits to effectively control the oscillatory dynamics of soliton breathers. Our manuscript is organized as follows: in Section 2 we present the model used; in Section 3 we investigate the generation and dynamics of stable CS; in Section 4 we identify the control parameters which permit to trigger soliton breather oscillations, and we study the effect of pump pulse chirping on their dynamics; finally, in Section 5 we draw our conclusions.

* Corresponding author.
E-mail address: francescorinaldo.talenti@uniroma1.it (F.R. Talenti).

https://doi.org/10.1016/j.optcom.2023.129773
Received 30 May 2023; Received in revised form 19 July 2023; Accepted 20 July 2023
Available online 24 July 2023

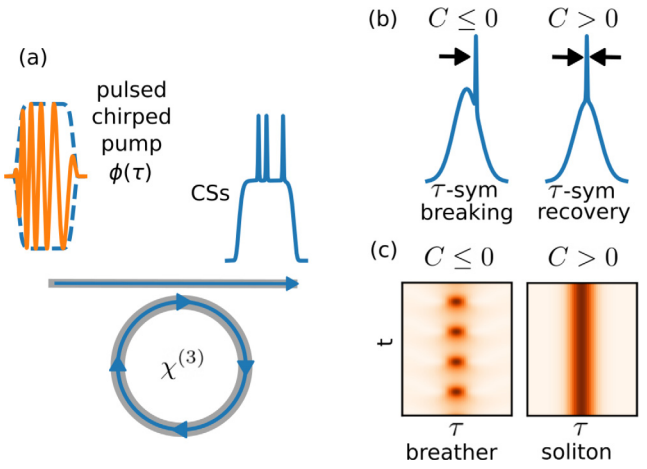

Fig. 1. (a) Linearly chirped, pulsed pumping scheme for Kerr CS generation; (b) Unchirped or negatively chirped ($C \leq 0$) pulsed pumping scheme may lead to temporal symmetry-breaking of the intra-cavity field. Time symmetry can be recovered by means of a positive chirp ($C > 0$) driving field. (c) Similarly, a positively chirped pump pulse may transform a soliton breather into a stable CS.

2. Super-Gaussian pumping scheme for Kerr cavity soliton generation

CS propagation is ruled by the coherently driven and damped 1-D nonlinear Schrödinger or Lugiato–Lefever equation (LLE). In normalized units and with anomalous group-velocity dispersion, it reads as [26–28]:

$$\frac{\partial E(t,\tau)}{\partial t} = \left[-1 + i\left(|E|^2 - \Delta\right) + i\frac{\partial^2}{\partial \tau^2}\right] E + S(\tau) \quad , \tag{1}$$

where E is the intra-cavity field amplitude, and Δ is the laser/cavity detuning. The two time variables t (*slow time*) and τ (*fast time*) represent the two different temporal scales for the evolution of the mean field: across successive cavity round-trips, and within the cavity, respectively. Hence, τ is a physical time, whereas t is a fictitious continuous temporal variable that replaces the longitudinal spatial coordinate in an Ikeda map approach for describing temporal cavity dynamics [29]. Here we consider a super-Gaussian, linearly chirped pump pulse of the form:

$$S(\tau) = S_0 \exp\left(-\left[\frac{\tau^2}{2\tau_G^2}\right]^q - \frac{iC\tau^2}{2\tau_G^2}\right) , \tag{2}$$

where the repetition rate of the pump pulse train is synchronized with the cavity round-trip time t_R. S_0 is the driving field peak amplitude, τ_G is the pump pulse width, q is the super-Gaussian order and C is the chirp parameter, which quantifies the strength of the driving field's phase modulation.

The Kerr cavity chirped-pulsed pumping scheme is sketched in Fig. 1 (a). In the following, we will show how this allows for the generation of either multiple or single CSs, placed on top of a quasi-flat pulsed intracavity background. Interestingly, a properly phase-modulated pump may also permit to recover the broken τ-symmetry of the CS with respect to its background [11], as sketched in Fig. 1(b). Similarly, as we are going to show, breathing soliton oscillations can be stabilized by introducing positively chirped pump pulses (see Fig. 1(c)).

3. Cavity soliton regime

To see how the chirped pump pulse scheme of Fig. 1(a) may affect CS formation, we have simulated the dynamics of a nonlinear passive resonator, pumped by a square wave (super-Gaussian of 4th order) pulse. We also introduced a linear ramp of the cavity detuning $\Delta(t)$, lasting for 5×10^4 cavity round-trips. This permits to explore the parameter space spanned by S_0, Δ, and C. The evolution of the intra-cavity intensity with Δ is illustrated in the τ vs. Δ diagram shown in Fig. 2(a)–(d), for different values of the chirp parameter C (ranging from $C = -0.05$ to $C = 1$). The intensity profile of the driving field, and the corresponding phase profile as in Eq. (2) (i.e., $\phi = -C\tau^2/2\tau_G^2$) are sketched in Fig. 2 (e–f), respectively. Regardless of the value of the chirp parameter C, all of the typical stages of the CS-based frequency comb generation are present in Fig. 2: first, a modulation instability (MI) generated pattern appears; next, after a stage of build-up of the intra-cavity energy, field spikes are formed, and start to interact chaotically; finally, CSs emerge from chaos. Note that, differently from the typical CW pumping scheme, temporal patterns only exist in the quasi-flat region of the super-Gaussian (SG) pump plateau, which is delimited by the pump pulse duration (see gray dashed lines). We here focus on the CS regime. With a negative chirp (see Fig. 2(a) for $C = -0.05$), multi-CSs are typically generated from MI-induced chaos. The resulting CSs experience a drift towards the boundaries of the quasi-flat super-Gaussian background, depending on $\{S_0, \Delta, C\}$, and on the initial τ coordinate of the CS. As the cavity detuning grows larger, the CSs initially drift towards the edges of the pump pulse plateau, then flip their temporal trajectory and start to head towards the center of the pump pulse. This might cause a collision of CSs: as a result, the CS will merge into a single soliton. We may compare this dynamics with that obtained for an unchirped pump pulse ($C = 0.0$, see Fig. 2(b)). In that case, accelerated convergence of the CSs towards the center of the SG plateau is observed. The reason for this is that the trapping position of the CS is now obtained for lower values of $|\tau|$, for all dynamical sweeps of the cavity detuning. Still, we did not observe a clear convergence towards a τ-symmetric configuration. For a single CS, the chosen set of parameters leads to a τ-symmetry breaking, so that the stable trapping position of the CS is not centered at $\tau = 0.0$ [11].

We may generalize this conclusion by noting that, by positively chirping the driving field, we might expect to recover a symmetric configuration, where the CSs are pushed towards the center of the cavity. This process is depicted in Fig. 2(c) for $C = 0.15$, where we indeed observe a fast convergence of a multi-CS state towards a τ-symmetric single soliton configuration: CSs generated from chaos drift rapidly towards $\tau = 0.0$, eventually colliding and merging into a single CS. For larger C values (e.g., $C = 1.0$), the convergence is even faster, so that a single CS regime emerges quite immediately from chaos, as illustrated in Fig. 2(d).

The CS trapping position is related to the phase modulation of the driving field. Pump pulse chirping introduces a τ-dependent cavity phase detuning: as a result, CSs are attracted to the points in time with the largest effective detuning. Thus, the effective dynamical potential which is induced by a chirped pump generates local extrema of the cavity detuning. These correspond to a specific τ-position, where the CSs are trapped [11,12]; this situation is analogous to the case of using a bichromatic CW pump [30].

In our case, there are two main contributions to the dynamics of the CS drift. First, and above a certain pump threshold power, amplitude modulation of the pump shifts the generated CSs at specific values of the inhomogeneous background field. Second, with pure phase modulation the CSs are always attracted to maxima or minima of the driving field. When considering a chirped super-Gaussian pump, there is a coexistence of both amplitude and phase modulation. The strength and sign of the chirp concur in determining the attraction/repulsion among different CSs, and their temporal drift with respect to the center of the pump pulse.

Thus, once the other dynamical parameters are fixed, the trapping position of the CS is uniquely determined by the value of C [14,31]. This permits to use the pump chirp as a means to control the CS generation and dynamics. Interestingly, by increasing the strength of the pump phase modulation, we observed a faster convergence towards the generation of a single CS per round-trip. As a consequence, pump pulse chirping is a simple scheme for the deterministic generation of a

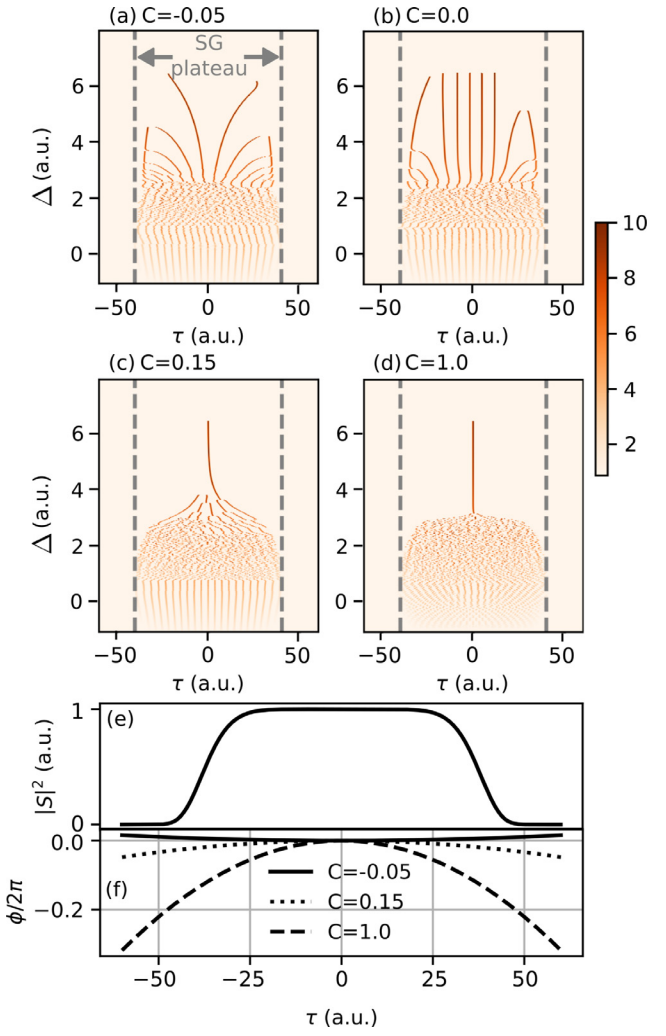

Fig. 2. The intra-cavity power from adiabatic sweeps of the cavity detuning, for different values of the chirp parameter C. Referring to Eqs. (1)–(2), we set $S_0 = 2.3$, $q = 4$, $\tau_G = 30$; the cavity round-trip time is t_r=120. Gray dashed lines delimit the extent of the super-Gaussian plateau, whose boundaries are defined by the pump pulse full width at half maximum (FWHM) (i.e. at $\tau \sim [-40.0, 40.0]$). In (e) we report the normalized intensity profile of the driving field, and in (f) we show its phase profile ϕ, for different values of the chirp parameter C.

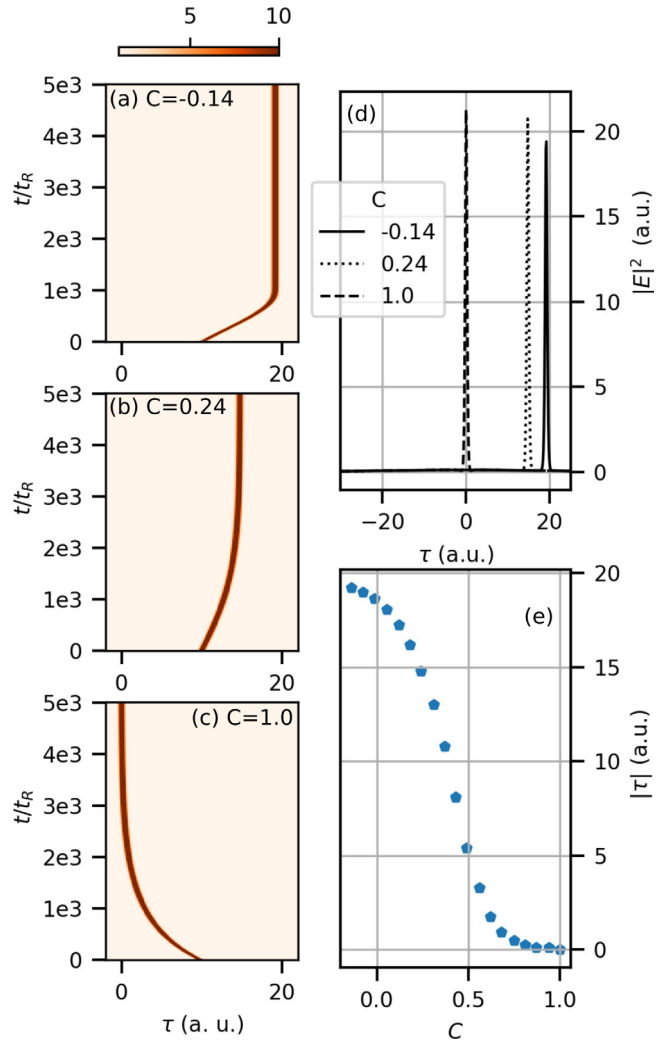

Fig. 3. Soliton drift dynamics: we consider a soliton initially located at $\tau_0 = 10.0$ and driven by a chirped pulse in a LLE system. On the left, we report the color-mapped field dynamics considering $C = -0.14$ (a), $C = 0.24$ (b), and $C = 1.0$ (c). In (d) we show the steady-state intra-cavity field, and in (e) the trapping fast time position $|\tau_S|$ of the CS, vs. the chirp parameter. For this set of simulations, we fix $\{S_0, \Delta, \tau_G\} = \{3.5, 10.0, 30\}$.

single CS within a large mode-locking range. The contour plots of the intracavity power in Fig. 2 show the presence of different regimes for the CS drift dynamics and its temporal trapping positions. The latter can be easily computed via direct numerical simulations with different values of C. In order to do so, let us consider the case of a Gaussian ($q = 1$) pump pulse, with the same pulse width ($\tau_G = 30$) but with a different value of its amplitude ($S_0 = 3.5$). In this situation, there exists a threshold $\Delta < \Delta_{thr}$, such that the CS starts to exhibit oscillatory behavior. We will return to the details of this breathing dynamics in the next section. For the moment, let us consider a sufficiently large value of the detuning ($\Delta = 10.0$), so that no breathing behavior is observed.

For the initial condition of our simulations, let us consider the sech-shaped soliton [11,30,32]:

$$u_0(\tau) = \sqrt{2\Delta}\,\mathrm{sech}\left((\tau - \tau_0)\sqrt{\Delta}\right), \tag{3}$$

where the stable τ-position is determined by the strength of both phase and amplitude modulation [15]. The reason of using the ansatz (3) is that u_0 corresponds to an exact solution of the LLE, whenever the driving field also equals u_0. We fixed the initial CS position $\tau_0 = 10$, and performed numerical simulations for different values of C. The results of this analysis are illustrated in Figs. 3(a)–(c) for $C = -0.14$, 0.24, and 1.0, respectively. In these figures, we plot the intra-cavity power $|E(\tau, t)|^2$: as can be seen, a slow t-evolution of the CS τ-position is observed.

For a negative chirp (see Fig. 3(a) for $C = -0.14$), a soliton which is initially located at $\tau_0 = 10$ is delayed from the center of the Gaussian background pulse, until it reaches a stable trapping position on the trailing edge of the pump pulse. This is a limit case, for which CSs can be sustained by this dynamics. For more negative C values, the CS escapes from the Gaussian background and disappears.

On the other hand, when C takes on positive values the opposite trend is observed. For $C = 0.24$ (see Fig. 3(b)), the CS is still delayed, but with a reduced rate: moreover, the CS reaches its final trapping position at a smaller time shift from the pump pulse center. Finally, Fig. 3(c) shows that, for $C = 1.0$, the CS accelerates towards the center of the Gaussian background, until the τ-symmetry is completely recovered.

The steady-state power profile of the intracavity field, for all previously discussed cases, is illustrated in Fig. 3(d). In general, by controlling the value of the chirp parameter C, one may continuously adjust the τ-trapping position of the CSs. To demonstrate this, we performed a set of simulations for different values of the chirp parameter (within

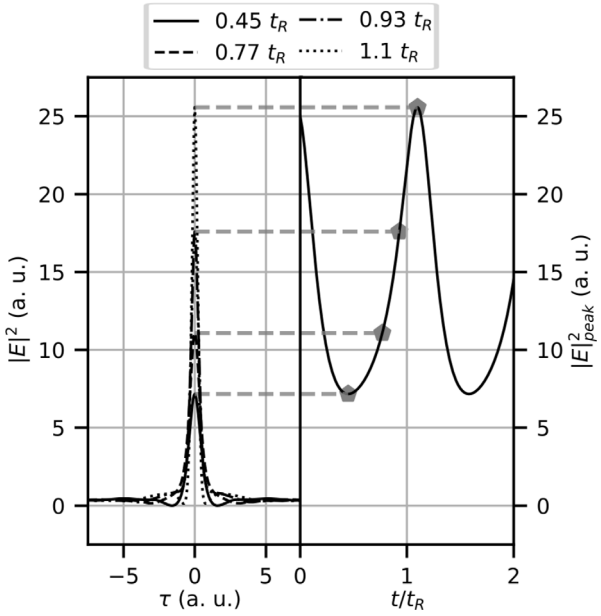

Fig. 4. Breather oscillatory dynamics. On the left panel, we report four different snapshots of the breathing soliton which is located on top of a Gaussian background, and oscillating between two constant extrema, in a stable oscillatory condition. For each snapshot, we report the corresponding slow time t coordinate in units of t_R. Referring to Eqs. ((1),(2)), we consider the values: $\Delta = 6.5$, $S_0 = 3.5$, $\tau_G = 60$, $C = 0$ and $q = 1$. In the right panel, we report the oscillations of the soliton peak intensity.

the interval $-0.14 \leq C \leq 1.0$), and we obtained the corresponding final CS trapping positions: these results are shown in panel (e). By tuning C, one may completely control not only the CS trapping position but also its drift. Indeed, the CS drift velocity v at τ_0 depends on the first τ derivatives of the phase and amplitude of the driving field. A general expression for this velocity takes the form [15]:

$$v(\tau_0) = a(S_0, \Delta)\frac{\partial}{\partial\tau}\phi(\tau_0) + b(S_0, \Delta)\frac{\partial}{\partial\tau}Re\{S(\tau)\}(\tau_0) \quad , \tag{4}$$

where the coefficients a and b uniquely depend on the pump amplitude and the detuning parameters [15]. With $a > 0$ being strictly positive for phase modulations, and $\partial\phi/\partial\tau = -C\tau/\tau_G^2$, we can find the C values for which the drift velocity vanishes at $\tau = \tau_0$.

In conclusion, the chirp parameter C is able to completely control the Kerr CS dynamics (i.e., its drift velocity and, consequently, its convergence towards the stationary state), once that the other cavity parameters are fixed [14,31].

4. Breather regime and chirp stabilization

Generally, in order to increase the complexity of a physical nonlinear system, it is sufficient to increase its total amount of energy. In our case, this can be obtained either by increasing the pump amplitude or by decreasing the laser/cavity detuning. While doing that, we may observe the emergence of multiple steady-states which can be static or dynamic. A typical example of the latter is the breathing soliton, or simply breather, whose oscillatory dynamics are sketched in Fig. 4. Here we consider the same set of parameters of the previous section ($S_0 = 3.5$, $C = 0$), except for the cavity detuning, which is lowered to $\Delta = 6.0$, thus reaching a Hopf instability regime where CSs start to oscillate. This breathing oscillation is shown in the right panel of Fig. 4, while on the left panel we report four different snapshots of this oscillation for different values of t. By fixing the input power to $S_0 = 3.5$, and sweeping both Δ and C, the CS dynamics may become more complex, as illustrated in Fig. 5, where we depict static CSs in (a), breathers in (b) and drifting breathers in (c).

At this stage, it is interesting to study in more detail the effect of pump chirp C on the CS dynamics, in order to implement a chirping technique that is capable of managing the emerging physics. In what follows, we show how a properly phase-modulated pump may affect, and eventually stabilize, the oscillatory dynamics of the resulting system.

In order to do so, first we performed a cavity scan with an unchirped pump and a linear ramp of the cavity detuning. We kept fixed $\{S_0, C, \tau_G\}$={3.5, 0.0, 30.0}, while spanning Δ from 4 to 16, and calculated at each t-instant the dynamical solution of the LLE-system of Eqs. (1)–(2). Moreover, we considered that, initially, the CS is centered at $\tau_0 = 0$. These results are illustrated in Figs. 6(a)–(b).

For exploring the upper single CS solution branch, we performed two sweeps, first with a negative detuning ramp, and the second with a positive detuning ramp, while starting in both cases from $\Delta = 10.0$. Fig. 6(a) shows the results of these scans in a intra-cavity power $|E(\Delta, \tau_{peak})|^2$ vs. $\Delta(t)$ diagram. For $\Delta = 4.0$, the system is chaotic (see blue shaded area), and thus $|E(\Delta, \tau_{peak})|^2$ oscillates rapidly, until reaching the threshold which is marked by the (i)-vertical dashed line. This line marks the lower limit of the breathing regime. The breathing region is delimited by markers (i–ii), and it is shaded in orange. Here the breather oscillates between minimum and maximum fixed values. Markers (ii–iii) delimit the CS regime (green shaded area), where the CSs are static, i.e. they do not oscillate. The (iii)-vertical line delimits the collapse of the system onto the quasi-homogeneous branch of solutions (red shaded area), which represents a deformation of the pulsed pump.

In Fig. 6(b) we report the peak intra-cavity power as a function of Δ. This diagram was computed by means of a path-numerical continuation of the steady-state CS solution (red dotted line); the linear stability of the corresponding solutions is depicted by using black solid and dashed lines for stable and unstable states, respectively. This approach allows us to compute the middle CS unstable branch, which is not reachable by direct numerical simulations. Our linear stability analysis reveals the onset of a Hopf bifurcation (see marker (ii) of the previous panel), from which breathers arise.

The typically nonlinear bistable behavior of the system can be observed by dynamically scanning the lower branch of quasi-homogeneous solutions. While sweeping the detuning, starting from $\Delta(t_0 = 0) = 10$, the system follows the upper branch of stationary solutions until reaching the fold bifurcation, or turning point, f', and then collapses onto the lower stable branch. On the other hand, when sweeping the detuning from values larger than (iii), and with a negative ramp (i.e. $\partial_t\Delta < 0$, [see green solid line]), the system stays on the lower quasi-homogeneous solution branch until reaching the other turning point f'', where the system jumps to the upper branch of solutions.

We may now generalize the study by sweeping the cavity with a chirped Gaussian driving field, considering values from $C = 0.0$ to $C = 400.0$. Always referring to Fig. 6, the peak powers of the intra-cavity field are reported in panel (c), while in (d) we report the extrema of the breathing oscillations. The raw data acquired in the numerical simulations (panel (c)), indicate that the chaotic region tends to be stabilized by the chirping effect. From a zero chirp, where the (i)-point delimits the passage from chaos to breathing dynamics at $\Delta_i > 4.0$, the Δ coordinate of (i) decreases to values $\Delta_i < 3.0$, when considering a high phase-modulated pump ($C = 400$). Similar considerations can be made for the point (ii). The shift of points (i-ii) vs. C is sketched in panel (e). The shift of (ii) implies the stabilization of the breather oscillations, resulting in a broader stable CS regime. The shift of point (i) means that the chaotic region shrinks and that chaos is suppressed for a wide range of detuning.

In general, the larger C, the more the breathing oscillations tend to be stabilized. For larger C values, the Hopf lobes shrink (panel (d)), meaning that the amplitude of the breathing oscillation decreases. Finally, we highlight in panel (f) the impact of chirping on the longitudinal breathing oscillation period. Here we report the two extreme

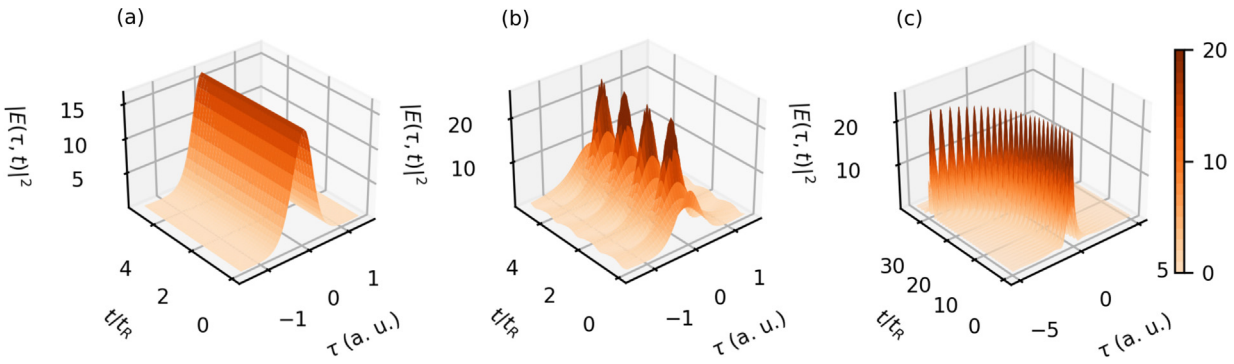

Fig. 5. Typical dynamical representation of a soliton (panel (a), $\{S_0, \Delta, C\} = \{3.5, 10.0, 1.0\}$), a breather (panel (b)), $\{S_0, \Delta, C\} = \{3.5, 6.0, 1.0\}$ and a drifting breather (panel (c)), $\{S_0, \Delta, C\} = \{3.5, 6.0, -0.5\}$.

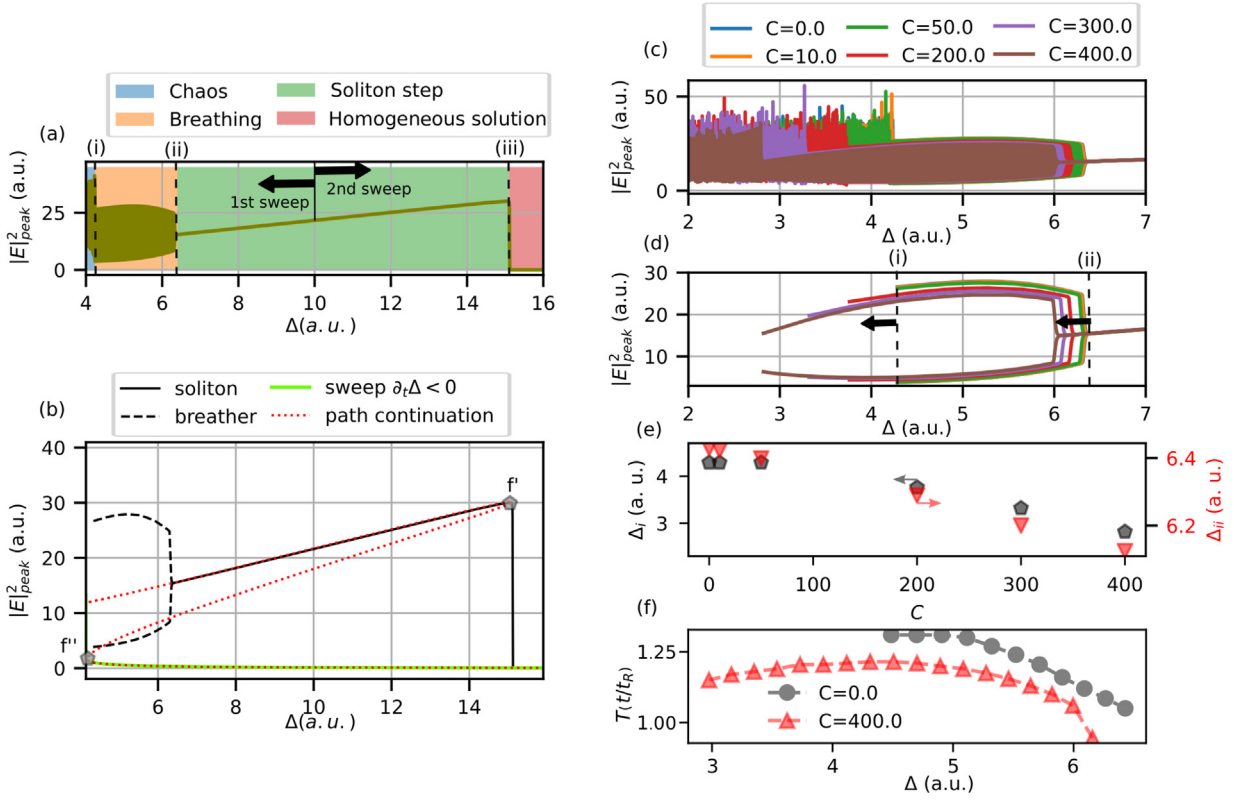

Fig. 6. Cavity sweeps where a pulsed driving field triggers the CSs dynamics. In (a) and (b) we consider an unchirped (C=0) driving field. In this case, we performed a dynamical sweep with a positive ramp of detuning, and we report the intracavity peak power. In (a), we report the raw data, while in (b) we show the periodic extrema of the breather oscillations. We also performed a negative ramp of the detuning (sketched in green), and we compare the simulated dynamics with the numerical solutions found by means of the path continuation theory (red dotted line). In panels (c–f) we study the effect of chirping, considering chirp values ranging from $C = 0.0$ to $C = 400$. Again, we report the raw data of the peak soliton power (c) and the breather extrema (d). In (e) are reported, for each case, the $\Delta_{i,ii}$ coordinates delimiting the endpoints of the breathing regime. In (f) we show the oscillation period in the breathing regime, for the two extreme cases studied, i.e. $C = 0.0$ and $C = 400.0$.

cases studied (i.e. $C = 0.0$ and $C = 400.0$). We can observe that, as the phase modulation increases, the breathing period decreases: the approaching of the two extrema results in faster oscillations.

In summary, from panels (c-f) we may conclude that introducing a chirped pump pulse permits to stabilize the dynamics of breathers, which tends to converge to a stationary soliton state. The Hopf bifurcation shifts towards lower Δ values, so that the soliton regime broadens. Moreover, the breathing oscillations are weaker, since both the oscillation period and its amplitude decrease. We may finally observe that pump chirping tends to suppress chaos, since the chaotic regime is pushed towards lower Δ values, as the chirp C grows larger.

5. Conclusions

Inhomogeneous pumping schemes of nonlinear passive resonators have been extensively studied recently. The fast-time symmetry breaking of soliton-like solutions [11–13] represents a paradigm shift,

enabling complete control of the Kerr cavity solitons (CSs) drift dynamics [14,15,31]. Phase and amplitude modulation of the driving field could potentially represent a reliable scheme to trigger the deterministic generation of specific CS states, which represent dominant dynamical attractors of the system [17]. An equivalent approach is that of modulating the intra-cavity generated pulses. In this perspective, recent publications showed how the temporal manipulation of Kerr CSs can be obtained by inserting an electric-optic modulator in a nonlinear passive optical cavity, in order to trigger Bloch oscillations [33], or to build signal synthesizers [34]. In a high-energy nonlinear regime, where the complexity of the system increases, alternative pumping schemes might be useful to access specific cavity states. For example, the insertion of a parabolic potential reveals the existence and stabilizes periodic temporal patterns [22]. In strict analogy, the method that we have analyzed here can be viewed as a stabilizing technique for breathers or chaotic states. The effective physics is that of an effective parabolic phase potential, which provides a new degree of freedom for the manipulation of trapped optical pulses.

Declaration of competing interest

The authors declare that they have no known competing financial interests or personal relationships that could have appeared to influence the work reported in this paper.

Data availability

Data will be made available on request.

Acknowledgments

This work was supported by the ADD Sapiexcellence 2022 grant, the Marie Sklodowska-Curie Actions (101064614,101023717), and the Olle Engkvist Foundation (Grant No. 214-0328). We would like to dedicate this work to the memory of Maurizio De Rosa, friend, and colleague, who left us a priceless cultural and scientific heritage, towards the demonstration of $\chi^{(2)}$ cavity soliton sources.

References

[1] S. Wabnitz, Suppression of interactions in a phase-locked soliton optical memory, Opt. Lett. 18 (8) (1993) 601–603, http://dx.doi.org/10.1364/OL.18.000601, https://opg.optica.org/ol/abstract.cfm?URI=ol-18-8-601.

[2] F. Leo, S. Coen, P. Kockaert, S.-P. Gorza, P. Emplit, M. Haelterman, Temporal cavity solitons in one-dimensional Kerr media as bits in an all-optical buffer, Nat. Photonics 4 (7) (2010) 471–476, http://dx.doi.org/10.1038/nphoton.2010.120.

[3] Y. Geng, H. Zhou, X. Han, W. Cui, Q. Zhang, B. Liu, D. Guang-Wei, Q. Zhou, K. Qiu, Coherent optical communications using coherence-cloned Kerr soliton microcombs, Nature Commun. (2021) http://dx.doi.org/10.21203/rs.3.rs-314550/v1.

[4] Q. Wang, Z. Wang, H. Zhang, S. Jiang, Y. Wang, W. Jin, W. Ren, Dual-comb photothermal spectroscopy, Nature Commun. 13 (1) (2022) http://dx.doi.org/10.1038/s41467-022-29865-6.

[5] J.K. Jang, M. Erkintalo, S. Coen, S.G. Murdoch, Temporal tweezing of light through the trapping and manipulation of temporal cavity solitons, Nature Commun. 6 (1) (2015) http://dx.doi.org/10.1038/ncomms8370.

[6] S. Barland, J.R. Tredicce, M. Brambilla, L.A. Lugiato, S. Balle, M. Giudici, T. Maggipinto, L. Spinelli, G. Tissoni, T. Knödl, M. Miller, R. Jäger, Cavity solitons as pixels in semiconductor microcavities, Nature 419 (6908) (2002) 699–702, http://dx.doi.org/10.1038/nature01049.

[7] P. Del'Haye, T. Herr, E. Gavartin, M.L. Gorodetsky, R. Holzwarth, T.J. Kippenberg, Octave spanning tunable frequency comb from a microresonator, Phys. Rev. Lett. 107 (2011) 063901, http://dx.doi.org/10.1103/PhysRevLett.107.063901.

[8] T. Herr, V. Brasch, J.D. Jost, C.Y. Wang, N.M. Kondratiev, M.L. Gorodetsky, T.J. Kippenberg, Temporal solitons in optical microresonators, Nat. Photonics 8 (2) (2013) 145–152, http://dx.doi.org/10.1038/nphoton.2013.343.

[9] S. Wabnitz, Control of soliton train transmission, storage, and clock recovery by cw light injection, J. Opt. Soc. Am. B 13 (12) (1996) 2739–2749, http://dx.doi.org/10.1364/JOSAB.13.002739, https://opg.optica.org/josab/abstract.cfm?URI=josab-13-12-2739.

[10] E. Obrzud, S. Lecomte, T. Herr, Temporal solitons in microresonators driven by optical pulses, Nat. Photonics 11 (9) (2017) 600–607, http://dx.doi.org/10.1038/nphoton.2017.140.

[11] I. Hendry, W. Chen, Y. Wang, B. Garbin, J. Javaloyes, G.-L. Oppo, S. Coen, S.G. Murdoch, M. Erkintalo, Spontaneous symmetry breaking and trapping of temporal Kerr cavity solitons by pulsed or amplitude-modulated driving fields, Phys. Rev. A 97 (5) (2018) http://dx.doi.org/10.1103/physreva.97.053834.

[12] I. Hendry, B. Garbin, S.G. Murdoch, S. Coen, M. Erkintalo, Impact of desynchronization and drift on soliton-based Kerr frequency combs in the presence of pulsed driving fields, Phys. Rev. A 100 (2) (2019) http://dx.doi.org/10.1103/physreva.100.023829.

[13] H. Taheri, A.A. Eftekhar, K. Wiesenfeld, A. Adibi, Soliton formation in whispering-gallery-mode resonators via input phase modulation, IEEE Photonics J. 7 (2) (2015) 1–9.

[14] F.R. Talenti, T. Hansson, S. Wabnitz, Control of Kerr cavity soliton combs by chirped pumping, in: OSA Advanced Photonics Congress (AP) 2020, IPR, NP, NOMA, Networks, PVLED, PSC, SPPCom, SOF, Optica Publishing Group, 2020, p. JTu2D.4.

[15] M. Erkintalo, S.G. Murdoch, S. Coen, Phase and intensity control of dissipative Kerr cavity solitons, J. Royal Soc. New Zealand 52 (2) (2022) 149–167, http://dx.doi.org/10.1080/03036758.2021.1900296.

[16] F.R. Talenti, T. Hansson, S. Wabnitz, Novel generation schemes for stable soliton states in optical microcavities, in: 2022 Italian Conference on Optics and Photonics, ICOP, 2022, pp. 1–4, http://dx.doi.org/10.1109/ICOP56156.2022.9911742.

[17] M. Rowley, P.-H. Hanzard, A. Cutrona, H. Bao, S.T. Chu, B.E. Little, R. Morandotti, D.J. Moss, G.-L. Oppo, J.S.T. Gongora, M. Peccianti, A. Pasquazi, Self-emergence of robust solitons in a microcavity, Nature 608 (7922) (2022) 303–309, http://dx.doi.org/10.1038/s41586-022-04957-x.

[18] S. Wabnitz, Suppression of soliton interactions by phase modulation, Electronics Letters 29 (19) (1993) 1711–1713, https://digital-library.theiet.org/content/journals/10.1049/el_19931138.

[19] N.J. Smith, W.J. Firth, K.J. Blow, K. Smith, Suppression of soliton interactions by periodic phase modulation, Opt. Lett. 19 (1) (1994) 16–18, http://dx.doi.org/10.1364/OL.19.000016.

[20] L.A. Jiang, M.E. Grein, H.A. Haus, E.P. Ippen, H. Yokoyama, Timing jitter eater for optical pulse trains, Opt. Lett. 28 (2) (2003) 78–80, http://dx.doi.org/10.1364/OL.28.000078.

[21] F. Parmigiani, P. Petropoulos, M. Ibsen, D. Richardson, Pulse retiming based on XPM using parabolic pulses formed in a fiber bragg grating, IEEE Photonics Technol. Lett. 18 (7) (2006) 829–831, http://dx.doi.org/10.1109/LPT.2006.871848.

[22] Y. Sun, P. Parra-Rivas, M. Ferraro, F. Mangini, M. Zitelli, R. Jauberteau, F.R. Talenti, S. Wabnitz, Dissipative Kerr solitons, breathers, and chimera states in coherently driven passive cavities with parabolic potential, Opt. Lett. 47 (24) (2022) 6353, http://dx.doi.org/10.1364/ol.472900.

[23] E. Lucas, M. Karpov, H. Guo, M.L. Gorodetsky, T.J. Kippenberg, Breathing dissipative solitons in optical microresonators, Nature Commun. 8 (1) (2017) http://dx.doi.org/10.1038/s41467-017-00719-w.

[24] G. Xu, L. Hill, J. Fatome, G.-L. Oppo, M. Erkintalo, S.G. Murdoch, S. Coen, Breathing dynamics of symmetry-broken temporal cavity solitons in Kerr ring resonators, Opt. Lett. 47 (6) (2022) 1486, http://dx.doi.org/10.1364/ol.449679.

[25] Y. Sun, P. Parra-Rivas, M. Ferraro, F. Mangini, S. Wabnitz, Nonlinear dynamics of dissipative structures in coherently-driven Kerr cavities with a parabolic potential, 2023, http://dx.doi.org/10.48550/arXiv.2305.00487, arXiv:2305.00487.

[26] L.A. Lugiato, R. Lefever, Spatial dissipative structures in passive optical systems, Phys. Rev. Lett. 58 (1987) 2209–2211, http://dx.doi.org/10.1103/PhysRevLett.58.2209.

[27] A. Pasquazi, M. Peccianti, L. Razzari, D.J. Moss, S. Coen, M. Erkintalo, Y.K. Chembo, T. Hansson, S. Wabnitz, P. Del'Haye, et al., Micro-combs: A novel generation of optical sources, Phys. Rep. 729 (2018) 1–81.

[28] M. Haelterman, S. Trillo, S. Wabnitz, Dissipative modulation instability in a nonlinear dispersive ring cavity, Opt. Commun. 91 (5–6) (1992) 401–407.

[29] T. Hansson, S. Wabnitz, Dynamics of microresonator frequency comb generation: models and stability, Nanophotonics 5 (2) (2016) 231–243.

[30] H. Taheri, A.B. Matsko, L. Maleki, Optical lattice trap for Kerr solitons, Eur. Phys. J. D 71 (2017) 1–13.

[31] J. Pan, C. Xu, Z. Wu, J. Zhang, T. Huang, P.P. Shum, Dynamics of cavity soliton driven by chirped optical pulses in Kerr resonators, Front. Optoelectron. 15 (1) (2022) 14.

[32] S. Coen, H.G. Randle, T. Sylvestre, M. Erkintalo, Modeling of octave-spanning Kerr frequency combs using a generalized mean-field Lugiato–Lefever model, Opt. Lett. 38 (1) (2013) 37–39.

[33] N. Englebert, N. Goldman, M. Erkintalo, N. Mostaan, S.-P. Gorza, F. Leo, J. Fatome, Bloch oscillations of coherently driven dissipative solitons in a synthetic dimension, Nat. Phys. (2023) 1–8.

[34] Y. He, R. Lopez-Rios, U.A. Javid, J. Ling, M. Li, S. Xue, K. Vahala, Q. Lin, High-speed tunable microwave-rate soliton microcomb, Nature Commun. 14 (1) (2023) 3467.